https://doi.org/10.5194/tc-2020-315
Preprint. Discussion started: 29 October 2020

The Cryosphere Discussions

Estimation of degree of sea ice ridging in the Bay of Bothnia based on geolocated photon heights from ICESat-2

Renée Mie Fredensborg Hansen[1,2], Eero Rinne[1], Sinéad Louise Farrell[3], and Henriette Skourup[2]

[1]Finnish Meteorological Institute, Marine Research, Erik Palménin aukio 1, 00560 Helsinki, Finland
[2]DTU Space, Geodesy and Earth Observation, Elektrovej Building 328, 2800 Kgs. Lyngby, Denmark
[3]University of Maryland, Geographical Sciences, 2181 LeFrak hall, College Park, MD20740, United States

Correspondence: Renée Mie Fredensborg Hansen (renee.fredensborg@fmi.fi)

Abstract. The ability to provide ice navigators with reliable and timely information on sea ice conditions is crucial to ensure safe passage through rapidly changing ice-covered waters. Degree of ice ridging (DIR) is a particularly useful parameter for ice navigators, as it provides an idea of how difficult it is to navigate through an area based on e.g. sail heights and distribution of sea ice ridges. DIR estimates are included in ice charts of the Baltic Sea, and are based primarily on *in situ* observations from an active icebreaker fleet. DIR may also potentially be estimated from satellite observations, and warrants further investigation. Here, we present a comparison of Ice, Cloud and land Elevation Satellite-2 (ICESat-2) geolocated photon heights and operational ice charts from the Finnish Ice Service in the Bay of Bothnia in spring 2019. We show that ICESat-2 (IS2) retrievals from ice areas with different ridging characteristics, more precisely DIR, differ significantly. Thus, we suggest that IS2 data can be of benefit to international ice services, especially if a time critical photon height product were to be made available. Furthermore, we show that the difference between highest and mean photon elevations (elevation anomalies) of IS2 correspond to expected ridge sail heights in our study area. Our study is one of the first steps in creating sea ice applications beyond the traditional goal of freeboard and thickness retrieval for IS2.

1 Introduction

Rapid changes in the sea ice conditions cause challenges to ship navigation (Duncan et al., 2018). Thus, the ability to provide users with reliable and timely information of the ice conditions is time-critical and of high priority (Gegiuc et al., 2018). Some of the most important sea ice parameters for ice navigation are the ice extent, stage of development, concentration, thickness, and the amount and location of ridged ice. The amount and location of ridged ice is important, since navigation through heavily ridged sea ice is difficult and potentially dangerous (e.g., Kovacs et al., 1973; Gegiuc et al., 2018; Goerlandt et al., 2017; Ronkainen et al., 2018).

The Baltic Sea extends from 54 to 66° N with a total area of 422 000 km^2 (Ronkainen et al., 2018). The seasonal ice cover usually appears in early November and persists until mid-May with the largest extent between January and March (Goerlandt et al., 2017). Wintertime shipping through the ice covered sea into Northern harbours requires timely and accurate ice information provided by the Finnish and Swedish ice services. This information is provided in the form of daily operational ice charts. Generally, the sea ice in the Baltic Sea is divided into fast and drift ice. Fast ice occurs in coastal regions and archipelagos, and

https://doi.org/10.5194/tc-2020-315
Preprint. Discussion started: 29 October 2020


The Cryosphere Discussions
Open Access
EGU

grows thermodynamically as it is attached to the coast where it remains stationary (Ronkainen et al., 2018). Wind and currents drive the drift ice by moving the ice floes. Sea ice areas with divergent motion forms cracks and leads in the ice cover, and areas with convergent motion results in formation of rafted ice and ice ridges (Gegiuc et al., 2018).

Daily ice charts of the Baltic Sea ice are prepared by the Finnish Ice Service (FIS) analysts and provide a source of information on the ice conditions. The charts partition the ice cover into polygons to which ice types and other properties are assigned. Parameters assigned to each polygon are ice concentration, average level-ice thickness, maximum and minimum level thickness and the degree of ice ridging (DIR). Satellite Synthetic Aperture Radar (SAR) imagery are the main data source for ice charts, but DIR is based mostly on visual icebreaker observations. This is because DIR is designed to be a representative description of the navigational difficulties from the point of view of the navigator (Ronkainen et al., 2018).

The National Aeronautics and Space Administration (NASA)'s Ice, Cloud and land Elevation Satellite-2 (ICESat-2) was launched on 15 September 2018 and builds upon the heritage of the Ice, Cloud and land Elevation Satellite (ICESat) mission (Neumann et al., 2019; Abdalati et al., 2010). One of the primary mission objectives for ICESat-2 (IS2) is to estimate the thickness of sea ice and monitor any changes therein (Markus et al., 2017). The main payload of IS2 is the Advanced Topographic Laser Altimeter System (ATLAS), a photon counting laser system operated at 532 nm with a pulse-repetition frequency of 10 kHz (Kwok et al., 2019b). The ATLAS instrument employs a multi-beam configuration consisting of three pairs of beams (strong and weak beams) separated across-track by approximately 3 km and a pair spacing of 90 m (Brunt et al., 2019). The individual footprints of $\sim$17 m are separated by $\sim$0.7 m (Kwok et al., 2019a). The novel beam-pair photon-counting approach overcomes the limitations of its predecessor ICESat, as it allows for the determination of local across-track variations, e.g. sea surface height measurements in open, often narrow, leads required for sea ice freeboard and ice thickness retrievals (Markus et al., 2017). The dense surface coverage also allows for pressure ridge detection based on e.g. studies that used the photon elevations from Multiple Altimeter Beam Experimental Lidar (MABEL), an airborne simulator used to test the instrument theory and strategy of IS2 (Farrell et al., 2015). Furthermore, the first study using IS2 to estimate surface topography and ridges in the Arctic has recently been published (Farrell et al., 2020). IS2 is a novel instrument and we expect that there is a vast amount of information on sea ice in the data products not currently used due to lack of methodology. Developing such novel methodology is the key driver for this study.

This paper presents a feasibility study demonstrating the use of IS2 data (granules) to estimate sea ice ridging information relevant for ice navigation. Our study is based on four IS2 passes from early 2019 in the Baltic Sea. We compare IS2's Global Geolocated Photon Data (ATL03) product to ice charts from the FIS. We have chosen the Baltic Sea as our test area, since this is, to our knowledge, the only area covered by a dense time series of ice charts where ice ridging estimates are based on frequent reports from an active ice breaker fleet (WMO, 2010). We discuss the potential of IS2 to complement satellite SAR imagery which is widely used by ice services, and the potential benefits of a time-critical IS2 product to international ice services.

https://doi.org/10.5194/tc-2020-315
Preprint. Discussion started: 29 October 2020

The Cryosphere Discussions
Open Access
EGU

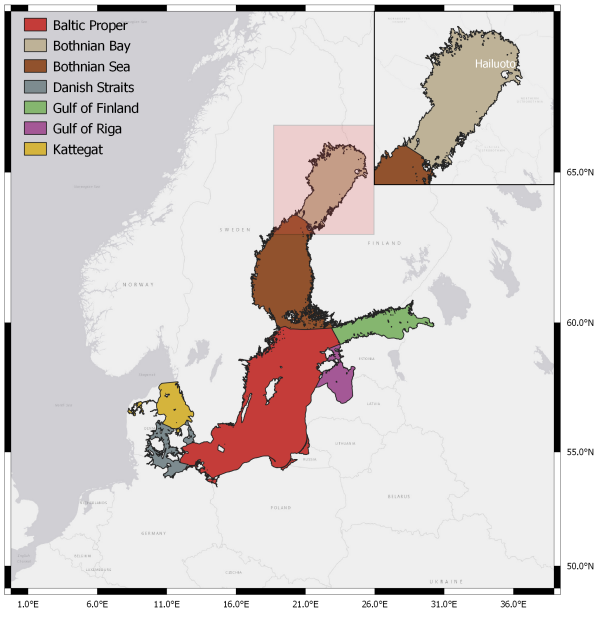

Figure 1. The Baltic Sea and its sub-basins as defined by the Baltic Marine Environment Protection Commission – Helsinki Commission (HELCOM) available at: http://maps.helcom.fi/website/mapservice/ (Accessed 21 October 2020). A highlight of our study area, the Bay of Bothnia, is shown at top right with red square showing its location. Environmental Systems Research Institute (ESRI) World Base Light Grey is used for background map, available at: https://felix.rohrba.ch/en/download/2696/ (Accessed 21 October 2020).

2 Data and methods

Our study area (Fig. 1) is the northernmost basin of the Baltic Sea, the Bay of Bothnia, north of the sound of Quark at 63.5° N, during the ice season 2018–19. The ice winter of 2018–19 was mild with a maximum extent of the ice cover in the Baltic of 88 000 km^2 reached on 27 January. FIS classifies the winters as mild in the Baltic if the ice extent is below 115 000 km^2 (Ronkainen et al., 2018; BIM, 2019). The ship traffic was dense, where according to the Baltic Icebreaking Management (BIM), 1428 vessels were assisted during the 2018–19 ice season (27 December – 5 May) in the Bay of Bothnia (BIM, 2019). Even though the winter was mild, icebreakers frequently reported heavily ridged ice areas and rubble fields in February and March.

2.1 Ice charts and degree of ice ridging

FIS produces daily ice charts during the ice season. The ice charts are provided as both vector charts and gridded products that contain information on ice concentration, average thickness, minimum and maximum thickness, sea surface temperature and a numeral description of deformation known as DIR (Gegiuc et al., 2018). DIR classifies ice into six categories (from 0 to 5) denoting level ice (0), rafted ice (1), slightly ridged ice (2), ridged ice (3), heavily ridged ice (4), and brash barrier

https://doi.org/10.5194/tc-2020-315
Preprint. Discussion started: 29 October 2020

(5) (Ronkainen et al., 2018). The ice charts are based on satellite SAR, visible and infrared satellite imagery, sea ice models and *in situ* measurements including observations from ice breakers and coastal observations by volunteer ice observers (Berglund and Eriksson, 2015).

The quality and uncertainty of the ice chart depends partly on the quality of the SAR imagery, but also on the experience of the ice analyst, which both can result in inconsistencies in the final ice chart. Assigning a DIR value to each ice chart polygon is a complex process that requires a profound understanding of the current ice season and ice development (Gegiuc et al., 2018). Most importantly, routine reports from the Finnish and Swedish ice breaker fleets are used to estimate ridging. It should be noted that assigning one numeral to a large area of sea ice is necessarily a simplification – in reality the ice in the area is always a mixture of several ice types. We emphasise that the FIS ice chart carries more information than just that from satellite SAR imagery. Because the high number of vessels in the Baltic at all times, FIS ice charts utilise significantly more *in situ* knowledge than Arctic ice charts. During the ice winter 2018–19, FIS received 1628 ice information messages from ice breakers (BIM, 2019). For this reason they are used here as the reference data set.

DIR and satellite data have been compared to each other by Gegiuc et al. (2018). To build an automatic method to derive DIR from SAR imagery, they applied a random forest (RF) algorithm to dual-frequency (HH/HV) RADARSAT-2 SAR, where H denotes horizontal and V denotes vertical polarisation, and used the FIS ice charts as reference data. The results were promising when a significant amount of ridging had occurred, allowing for the ridging to strongly contribute to the texture of the SAR images. To the best of our knowledge, this is the only study that utilises satellite measurements to estimate DIR to supplement ice charting. Analogously, we investigate the possibility to estimate DIR from IS2.

2.2 The Ice, Cloud and Land Elevation Satellite 2 (ICESat-2)

IS2's main payload, the laser altimeter ATLAS employs a multi-beam configuration consisting of six beams (3 beam pairs with a strong and weak beam). The strong beams are $\sim$4 times the pulse energy of the weak (Kwok et al., 2019a). Left (of individual beam pairs imaginary centerline) beam is denoted GTL, and right beams by GTR. Number of specific beam pair (dependent on the orientation of the spacecraft) ranges from 1-3. The IS2 reference ground track (RGT) is a imaginary centerline of the ground track pattern of the multi-beam configuration, and it takes 91 days to sample all 1387 unique RGTs, fulfilling one full cycle (Brunt et al., 2019).

2.2.1 Global Geolocated Photons (ATL03) data product

In our study, we use the Global Geolocated Photons Level 2A Data Product (ATL03) from IS2. ATL03 is produced by combining the laser pointing vectors, the position of the IS2 observatory and the individual photon times of flight from ATL02 (Science Unit Converted Telemetry Level 1B Data Product) (Neumann et al., 2019). ATL03 includes the longitude (*lon_ph*), latitude (*lat_ph*) and World Geodetic System 1984 (WGS-84) ellipsoidal heights of the photons (*h_ph*) alongside a coarse discrimination of what is likely signal and what is background events (*signal_conf_photon*); a surface classification to identify land, ocean, land ice, sea ice and inland water (with surfaces overlapping by 20 km); geophysical corrections to be applied (Earth Gravitational Model 2008 (EGM2008) geoid (*geoid*), MOG2D dynamic atmosphere correction/inverted barometer as

https://doi.org/10.5194/tc-2020-315
Preprint. Discussion started: 29 October 2020

calculated by Archiving, Validation and Interpretation of Satellite Oceanographic data (AVISO) (*dac*) and ocean tide given by the GOT4.8 model (*ocean_tide*) and other parameters useful for higher-level products (Neumann et al., 2019).

The coarse discrimination of signal and background photons is based on generated along-track histograms. The identification of signal photon events is based on the location of regions where the photon event rate is significantly larger than the background photon event rate. All photons in a given bin are either classified as signal or background events. The planned data latency of ATL03 is 21 days, where latency is defined as approximate time from data acquisition to data products reaching end users in a suitable format (Brown et al., 2016).

We found four overpasses with clear sky conditions in our study region where IS2 measured ice areas that were marked as ridged (DIR2–DIR4) in the FIS ice charts on 1 February, 17 February, 23 March and 27 March 2019. Data from these dates are used in our study. The different DIR areas measured by IS2 as well as satellite ground tracks are shown in Sect. 3.1. DIR2 was sampled by IS2 on 1 February (a) and 17 February (b+c), DIR3 on 23 March (d) and 27 March (e) and DIR4 solely on 27 March (f), where (a)–(f) highlights how many sub-regions of data have been extracted from the different DIR zones at the specific dates.

2.3 Estimation of degree of ice ridging using ICESat-2 photons

Our hypothesis is that the areas of heavier ridging (high DIR) should be distinguishable within the ATL03 photon elevations since the heavier the ridging, the higher the ridge sail heights and thus a larger amount of the measured elevations should be higher than the elevation of level ice, when compared to areas with less ridging. This assumption is only based on the amplitude of the ridging in the areas and not on spatial parameters, e.g. ridge density. Thus, we investigate the distributions of the photon elevations over a segment of $N = 150$ photons. This corresponds to segments of approximately 17 m in length (based on measurements of one strong beam (GT3L) from 17 February 2019, but exact segment length varies with the amount of geolocated photons reflected from the surface). To eliminate sea level changes and differences between actual sea surface height and the geoid, we subtract the mean elevation of the segment from all of the photon elevations within that segment. We filter the ATL03 photons by selecting photons of only high signal confidence and apply the geophysical corrections. The geophysical correction is part of the pre-processing filtering. We also discarded all measurements that deviated from the geoid elevation by more than 3 m.

We look first at the elevation distribution per segment, where the highest elevation are relative to the mean elevation of the segment. We find that the distribution of the relative elevations differ with respect to the different DIR zones (Fig. 2a), but with significant overlap. However, when we look only at the highest 20 %, 10 %, 5 % or 1 % of the relative elevations (Fig. 2b–e), the separation between the DIR zones increases significantly. Looking only at the high end of the distributions corresponds to looking at only segments where there is significant height difference between the highest and the mean elevation – that is, segments with tall ridge sails. This suggests that DIR in our study area can be estimated from ATL03, simply by looking at the highest percentile of relative elevations. This relative elevation or elevation anomaly, h_a, of the highest elevation within a

https://doi.org/10.5194/tc-2020-315
Preprint. Discussion started: 29 October 2020

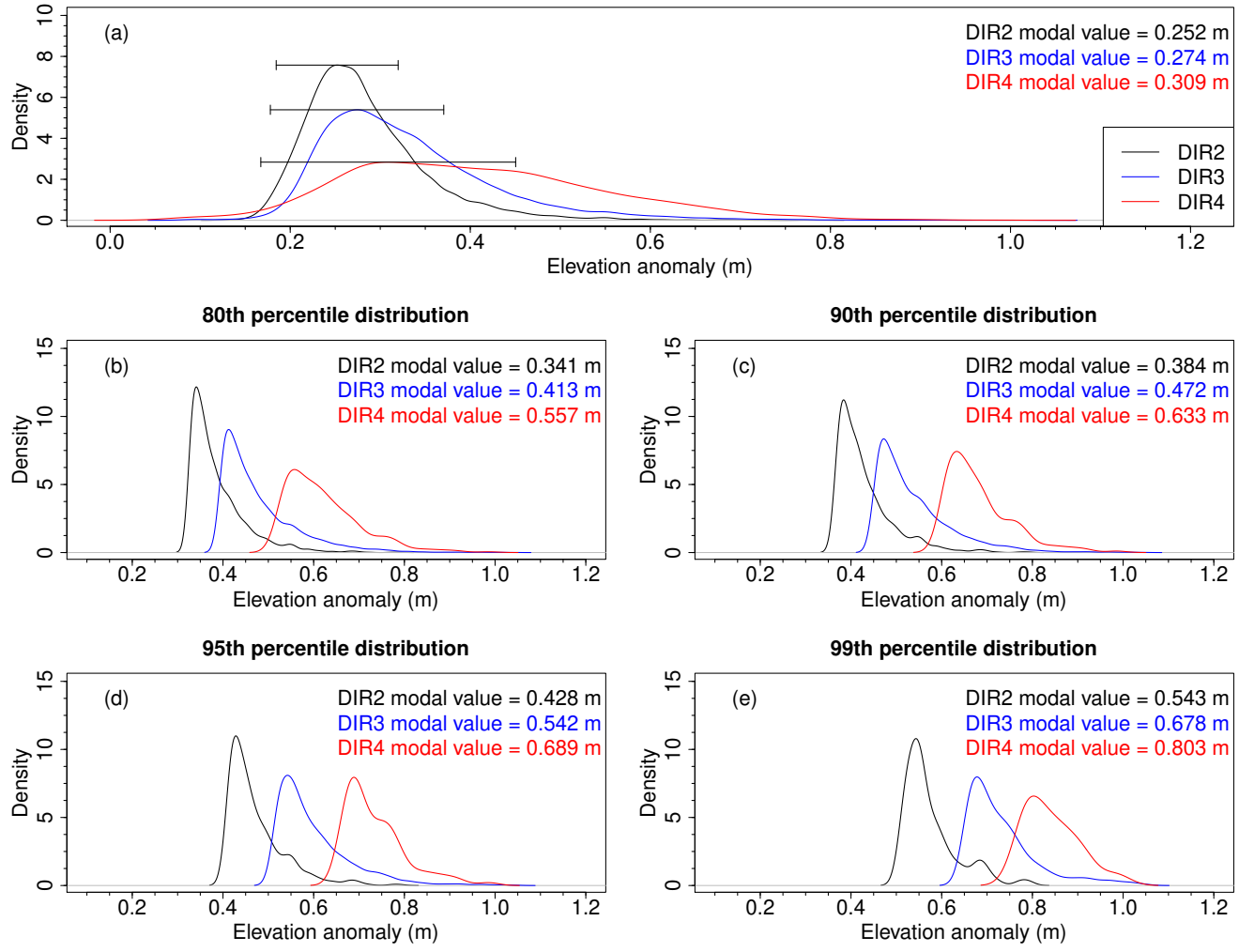

Figure 2. Distributions of elevation anomaly (h_a) to estimate different degree of ice ridging (DIR) zones. DIR2, DIR3 and DIR4 are shown in black, blue and red, respectively. (a) distributions of h_a of all segments from the different DIR zones with standard deviation indicated by horizontal markers, (b) distributions of 80th percentile values of $N = 150$ photon segments (the 20% highest values), (c) the 90th percentile values (10% highest values), (d) 95th percentile values (5% highest values), and (e) 99th percentile values (1% highest values). Modal value for each distribution are provided in the graphs.

segment of $N = 150$ photons subtracted the mean elevation of this segment, is defined as:

$$h_a = \sum_{N=1}^{150} h_{max} - h_{mean}, \tag{1}$$

where h_{max} is the highest elevation within the segment and h_{mean} is the average elevation of that particular segment.

https://doi.org/10.5194/tc-2020-315
Preprint. Discussion started: 29 October 2020

We built a simple threshold-based classification scheme to extract DIR values from IS2, based on the distributions in Fig. 2. While there is a clear separation already at 90 %, large overlaps remain between the distributions for DIR2 and DIR3 (Fig. 2c). This precludes the use of a simple threshold based interval to distinguish between the two DIR zones. For the 95 % percentile (i.e. the 5 % highest elevations) the overlap between the DIR zones is reduced (Fig. 2d), and thus classification more reliable. Since the distributions are skewed towards higher elevations, we use the mean absolute deviation (MAD) to estimate the thresholds instead of the classic standard deviation (SD). MAD is simply the median of the absolute deviations from the median and acts as a more robust dispersion/scale measure in the presence of outliers, whereas SD is especially affected by outliers (Leys et al., 2013). Estimations of mode, MAD and the given intervals for each DIR zone (modal $\pm$ MAD) using the 95th percentile data, are provided in Table 1. To exclude a gap between DIR3 and DIR4, a small adjustment (of $\leq$ 0.03 m), based on manual interpretation, is applied to the intervals.

Table 1. Estimated mode, mean absolute deviation (MAD) and intervals (thresholds) from 95th percentile (5 % highest values) of the elevation anomalies, h_a, for each DIR zone. The thresholds are given by the modal value $\pm$ MAD. Adjusted intervals are simply to exclude the gap between DIR3 and DIR4. Values in parenthesis show the elevation anomaly h_a using the 98th percentile, instead of the highest elevation, subtracted the mean (excludes $\sim$3 observations for each 150 photon segment), possibly useful for excluding possible noise measurements. The 98th percentile approach is discussed further in Sect. 3.2.

Ridging zone	Mode (m)	MAD (m)	Intervals (modal $\pm$ MAD) (m)	Adjusted intervals (m)
DIR2	0.43	0.05	0.39 – 0.48	0.38 – 0.48
	(0.33)	(0.05)	(0.28 – 0.37)	(0.28 – 0.37)
DIR3	0.54	0.06	0.48 – 0.60	0.48 – 0.60
	(0.42)	(0.05)	(0.37 – 0.47)	(0.37 – 0.49)
DIR4	0.69	0.06	0.63 – 0.75	0.60 – 0.75
	(0.55)	(0.05)	(0.49 – 0.59)	(0.49 – 0.59)

3 Results and discussion

3.1 Degree of ice ridging in the Bothnian Bay

Using our method, we classify IS2's geolocated photon heights into the different DIR categories and present the results in Fig. 3, together with the DIR zones provided by the FIS ice charts. As expected, IS2 photons classified as DIR2 (slightly ridged ice) occur in all FIS DIR zones simply because there are areas with smoother surfaces, i.e. level ice floes between ridges, in all zones. Similarly, IS2 derived values of DIR3 and DIR4 will also be seen in a DIR2 zone since even if the area has comparably little deformation, there may be individual ridges present. In other words, IS2 is able to distinguish features at much smaller scales than the resolution of an ice chart or indeed what is practical for tactical navigation.

https://doi.org/10.5194/tc-2020-315
Preprint. Discussion started: 29 October 2020

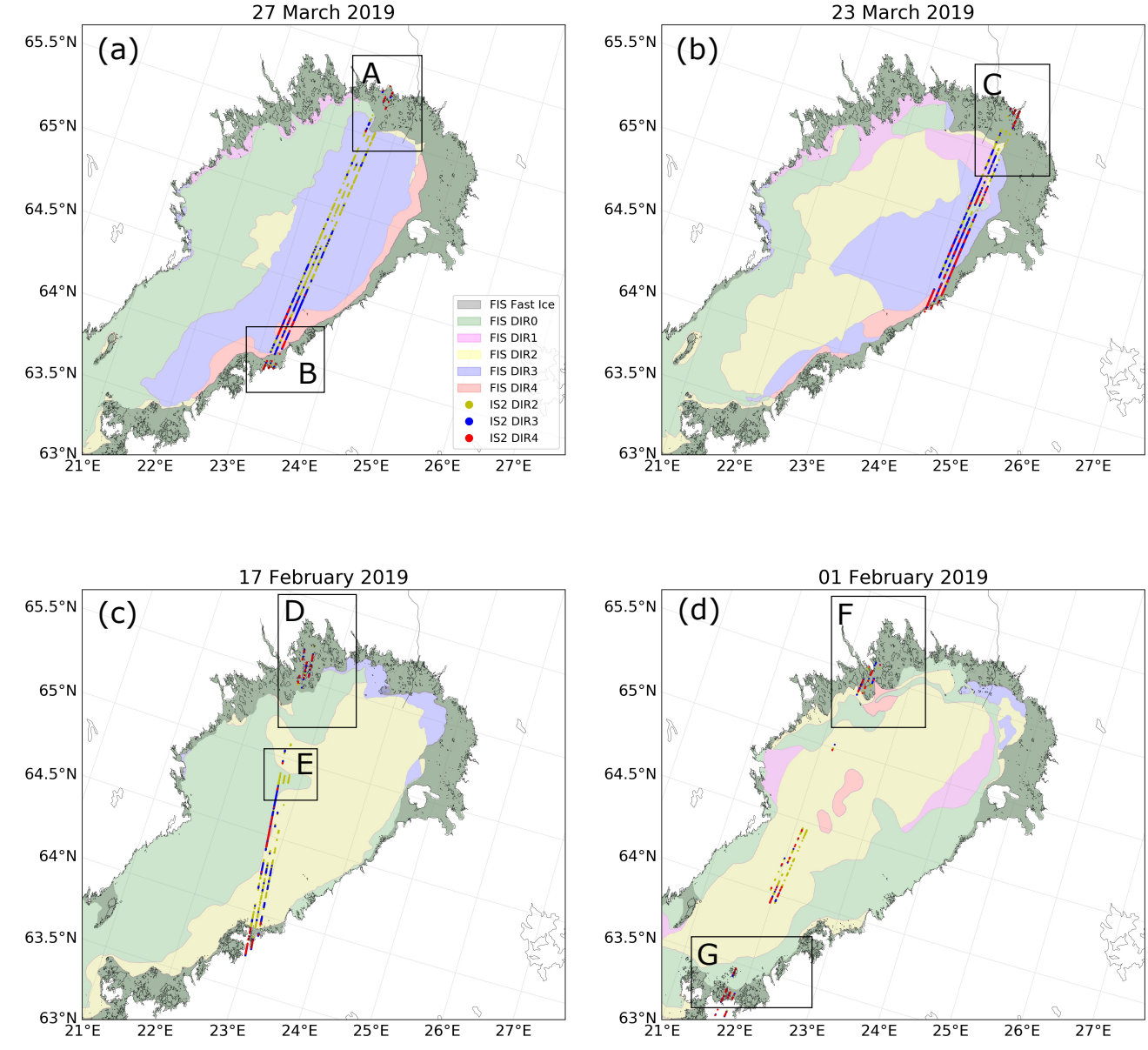

Figure 3. Categorised DIR data over four available days; (a) 27 March 2019, (b) 23 March 2019, (c) 17 February 2019 and (d) 1 February 2019. Contours show DIR polygons derived from Finnish Ice Service (FIS) ice charts, shown as; DIR0 (green), DIR1 (magenta), DIR2 (yellow), DIR3 (blue), and DIR4 (red). IS2 photon heights have only been classified for DIR2–DIR4, where several photon heights could be extracted from compared to DIR0–DIR1. Darker areas close to the coast denotes fast ice. A–G denotes different areas of interest mentioned in the text.

https://doi.org/10.5194/tc-2020-315
Preprint. Discussion started: 29 October 2020

The general behaviour of the distributions of IS2 DIR estimates follows the DIR zones from the ice charts. However, IS2 data carries much more information than just the overall DIR for the zone. As mentioned before, the ice chart DIR is a simplification, and in reality large areas that have been assigned to one single DIR are a mixture of several ice types. If ridge features are sparsely distributed and the area has a relatively large amount of open water, the zone will be assigned DIR2 by the FIS. This behaviour is seen in Fig. 3. For heavily deformed ice, Fig. 3a shows a cluster of IS2 classified DIR4 near and in the DIR4 zone of the ice chart. The distribution of IS2 DIR3 is also larger in the southern part of the track (near the border of DIR4) compared to the northern part in line with the ice charts. There is a large amount of IS2 DIR2 values in the DIR3 area suggesting that this part of DIR3 has less ridging. However, this is only based on an amplitude parameter and one track; the surrounding behaviour and conditions of the ice are not known and it is expected that DIR2 will be occurring throughout the DIR3 and DIR4 zones.

Fig. 3b seems to overall have more IS2 DIR4 values (even compared with Fig. 3a that actually encounters a region classified as DIR4). Since this track is close to the coast, more deformation is expected to occur due to the ice drift pushing ice floes towards the coast and fast ice, allowing for further deformation. What is also clear from all four days (Fig. 3a–d), is that when IS2 travels over fast ice regions, the DIR values are almost non-existent except for few segments close to the coast or over small islands (e.g. Region A–D, and F–G), thus caused by land contamination. This is expected, since regions of fast ice primarily consist of smooth level ice represented by small differences in the elevation anomalies. Furthermore, they have overall more snow on them than drift ice, smoothing the surface even further. For the Regions A–C (Fig 3a–b) and G (Fig. 3d) it is clear that there are few DIR values over fast ice and the ones that are detected are actually located over land. Region D and F (Fig. 3c–d) are behaving unexpectedly: there are significant DIR values which are not directly close to the coast (Region F has some coastal values, but mostly DIR2 values. This can be partly explained by the fact that it is very close to a DIR2 polygon or that the ice within this zone is slightly more deformed). Region D–E (Fig. 3c) shows higher DIR values (DIR3 and DIR4) in places that are not covered by a DIR zone or near the zone they are classified as. This could be caused by several things; it may be caused by photons within a segment, which are not surface photons but are instead caused by background sunlight. While the histogram approach mentioned in Sect. 2.2.1 keeps photons flagged as surface signal, the bins categorised as surface can still include some background photon events (if the background rate threshold is set too low), thus introducing a spread about the true surface elevation. Some of the photons may also be caused by a (low-laying) cloud cover interfering with the photons, and that has not been entirely filtered out in the high signal confidence pre-processing step. Furthermore, these may be proper measurements of ice surface, but with waves penetrating the sea ice increasing the surface roughness (specifically near Region E), but also land contamination could explain this (e.g. Region A–D, and F–G). Thus, should one automate this estimation of DIR values to use for daily ice charting purposes, it would be necessary to look into additional pre-processing steps to exclude the cloud-cover disturbed photons as it can affect the result. These events could possibly be assigned a measure of confidence to warn the ice analyst. This flag could also be applied to the DIR values that are affected by background photon events.

Furthermore, although DIR is not uniformly defined and is highly dependent on the ice analysts interpretation of the provided auxiliary data, such as icebreaker routine reports and SAR imagery, it is widely accepted that DIR is dependent on both amplitude (e.g. ridge sails) and spatial (e.g. ridge density) parameters. The results presented in Fig. 3 focus on the amplitude of

https://doi.org/10.5194/tc-2020-315
Preprint. Discussion started: 29 October 2020

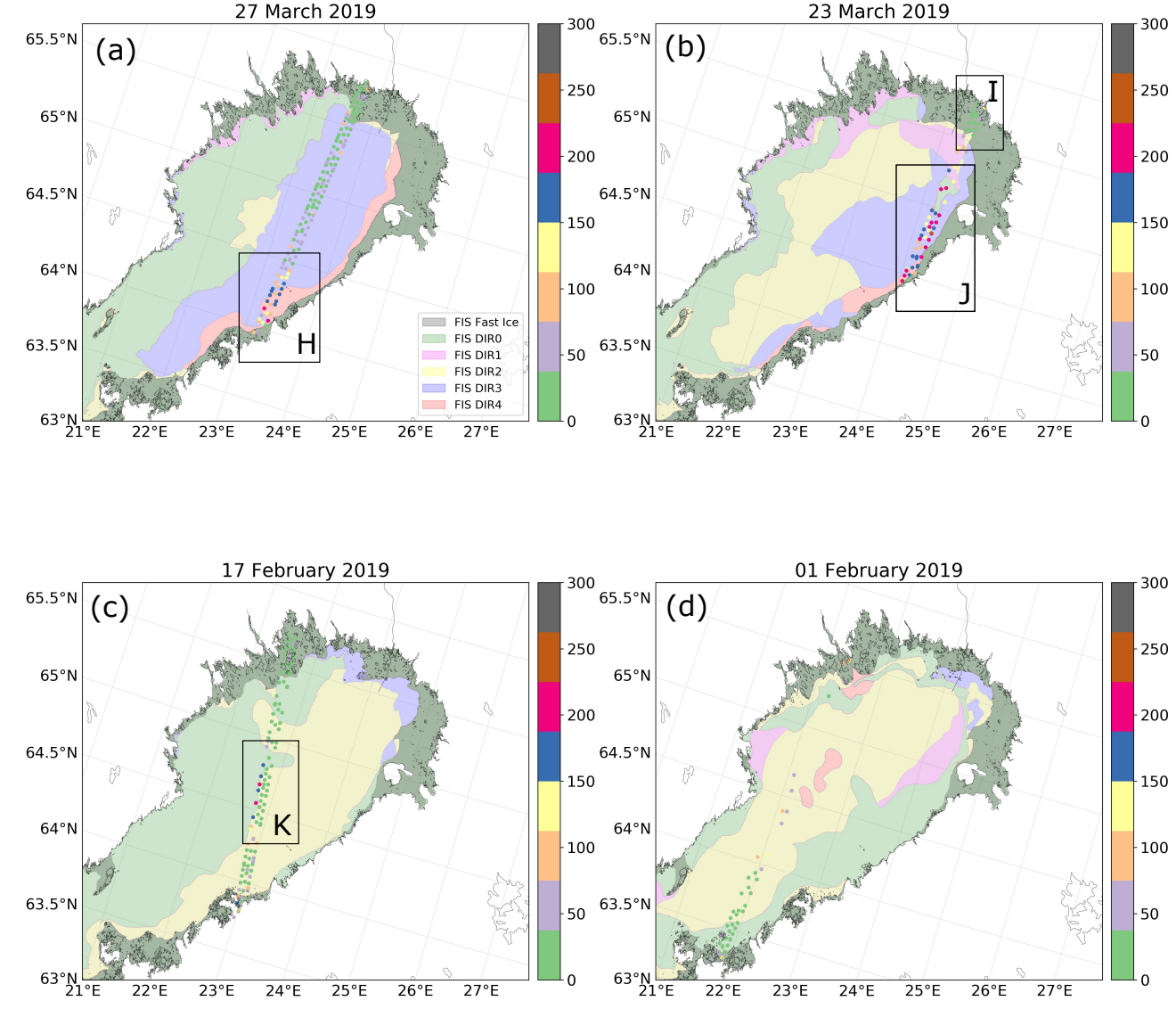

Figure 4. Counts of sails, within aggregated strips of 300 elevation anomalies, with values above 0.4 m acquired over four available days; (a) 27 March 2019, (b) 23 March 2019, (c) 17 February 2019, and (d) 1 February 2019, shown as; DIR0 (green), DIR1 (magenta), DIR2 (yellow), DIR3 (blue), and DIR4 (red). Darker areas close to the coast denotes fast ice. Colour-bar denotes amount of elevation anomalies, h_a, within a strip of 300 elevation anomalies above 0.4 m (cut-off height).

the sea ice roughness, and categorise DIR based on different amplitudes of ridge sail heights. However, the density of ridges is even more important to consider when navigating in ice-covered waters, since the higher ridge density, the harder it will be to navigate. To investigate the spatial distribution of ridges, we aggregate the elevation anomalies into strips of 300, thus covering

https://doi.org/10.5194/tc-2020-315
Preprint. Discussion started: 29 October 2020


The Cryosphere Discussions

an along-track distance of ∼5 km (assuming an average distance between the elevation anomalies, h_a, of 17 m). For the strips of 300 elevation anomalies, we count how many of these elevation anomalies exceed a cut-off height of 0.4 m, which would indicate a ridge in ice conditions encountered in the Baltic Sea (Lewis et al., 1993). The distribution of the amount of elevation anomalies above the cut-off height within a strip of 300 elevation anomalies is provided in Fig. 4. The small amount of counts (green and light purple colours, e.g. most of the track in Fig. 4a) represents a low ridge density, which is to be expected over lower DIR areas. The most interesting regions in Fig. 4 are denoted by letters H–K. In Region H, the higher ridge densities coincide with the highest DIR area; DIR4. The count for one strip of 300 elevation anomalies in Region H is around 150–200, which (by using a value of 180 counts per ∼5 km), is equivalent with 36 ridges per km. In the helicopter-borne electromagnetic (HEM) study utilised in Gegiuc et al. (2018) acquired primarily in March 2011, they obtained measurements in the Eastern Baltic that on average provided a ridge density for DIR4 of 21.5 ridges per km, and for the entire study, they encountered ridge densities in the range of 0–50 ridges per 1 × 1 nautical miles (NM) cells. Hence, the ridge densities for DIR4 obtained by IS2 is higher compared to the average of the HEM study, however not unlikely.

Region I shows very low count values, which is expected as the track covers fast-ice regions. This is also visible as low amplitudes (low ridge sail heights) in the same area in Fig. 3 (Region C). In Region J, there is a high spatial distribution of ridges with high sail heights (Fig. 3b) even though, according to the ice charts, the track does not coincide with DIR4 areas, i.e. the lowest DIR area the track coincide with is DIR3. However, the count values of Fig. 4b is higher, even higher than in Region H. Once more, this can be described by the sea ice measured (being mainly consolidated ice, when comparing to the FIS ice chart of 23 March 2019) is close to the coast and/or fast-ice, and the drift pattern in the Bay of Bothnia causing the sea ice to be pushed towards the eastern part of the Bay of Bothnia (near the island of Hailuoto, see Fig. 1 for precise location). Thus, the deformation of sea ice will be rougher – and most likely result in higher sails (Fig. 3b) – which will explain the higher counts in Fig. 4b. Finally, Region K shows a part of the track that suddenly experience high counts over low DIR areas, similar to the amplitude values in Fig. 3c. As has already been mentioned, this may be due to unfiltered photons from background sun events or cloud cover, i.e. noise photons. The affect of waves of significant height (above the cut-off height) has not been investigated, but should not be neglected, as studies have shown how IS2 photons can identify waves (e.g., Klotz et al., 2020; Horvat et al., 2020) and it is not unlikely, that waves will occur in this area and could be above the cut-off height, as the area (on the left of the yellow polygon in Fig. 4c) is classified as *very open ice* in the FIS ice chart.

Nonetheless, with the caveats above, this study shows the potential to use IS2 to supplement ice charting. In practise, this will require a near real-time or fast delivery photon product from IS2 that is currently not available. With the current 21 day latency for ATL03 (Brown et al., 2016), it cannot be used for daily ice charting which would be the optimal scenario.

3.2 Implications for ICESat-2 and future work

Our study is limited, as currently the IS2 data for 2019–2020 is not completely available yet. Even if it was, 2019–2020 was an exceptionally mild winter in our test area, and we would expect to find very few usable overpasses of IS2 over ridged ice. Throughout January to March 2019 only 25 granules of data passing the Bothnian Bay were available (which were either not or only partly affected by clouds to be removed by pre-processing steps). The Baltic sea is relatively small and located at

https://doi.org/10.5194/tc-2020-315
Preprint. Discussion started: 29 October 2020

comparably low latitudes, chosen for this study due to the availability of quality reference data. Nonetheless, this study shows the potential of IS2 data to supplement other sources of information for ice charting. Furthermore, with the expected increase of shipping in the Arctic as a response to the continuing melting of the sea ice cover (e.g., Melia et al., 2016), these results prove valuable not only for the Baltic ice services and ice charting, but also for international ice charting.

We have emphasised the need for a real-time or fast delivery photon product before, but it should be mentioned that even without time critical products, it would still be valuable to estimate the ice conditions for certain areas to use for planning purposes. An example of such planning would be compiling the statistical information on ice conditions required by the International Maritime Organisation (IMO) polar code to create a regional climatology (IMO, 2020).

Furthermore, we acknowledge a weakness of this method that results from the assumption that the highest photon elevations within a segment originate from a ridge sail. There is a possibility that they actually are due to a background sun light event or a cloud cover disturbed photons. Nonetheless, we find the overall elevation anomalies correspond with expected sail heights in the area, and it therefore seems likely that the confidence flag in the ATL03 product is of very good quality.

To evaluate the impact of possible noise photons being the highest measured elevation within a 150 photon segments, we investigated percentiles of the segments with mean value subtracted from each of the elevations, rather than the highest elevation subtracted the mean elevation (the elevation anomaly, h_a). Thresholds based on the 98th percentile of the mean subtracted the photon elevations rather than h_a (see Table 1) have similar intervals (about 0.10 m smaller of each interval), however the distribution of the classified DIR zones are similar to those of the elevation anomalies (as presented in Fig. 3). This suggests, that even by using only high-confidence photons and the highest value, in most cases the photons do in fact originate from the top of the ridges rather than noise photons. Hence, for ridge sails less than 1 m in height, the on-board filtration scheme of low, medium and high-confidence photons seems to keep only surface photons including photons originating from the top of the ridge sails, and successfully removes noise photons. Using the 98th percentile instead of h_a excludes approximately 3 photons per 150 photon segments, thus due to dead time and the single photon-counting method of IS2 (Neumann et al., 2019), the top of the ridge may not be included if the highest photon of the segment is excluded. However, the 98th percentile thresholds are also within range of average ridge sail heights determined by former studies (of 0.5–0.6 m, see Lewis et al. (1993) and Gegiuc et al. (2018)), and could be applied to work around the weakness mentioned of how the highest photons could be noise photons. Further validation of ridge sails and surface measurements of small-scale roughness, such as ridges in the Baltic Sea, observed by IS2 by comparing with airborne observations is encouraged.

We suggest that IS2 could be used by ice services should a near real-time or a fast delivery photon product become available. Currently, the data latency of the ATL03 data product is 21 days (Brown et al., 2016). Such information is of high priority, not only to support safe ice navigation in the Bay of Bothnia, but also across the Arctic given the increased presence of commercial vessels (even during winter-time) as a result of the decreasing sea ice cover to prevent accidents and potential pollution of the pristine Arctic environment. Due to along-track nature of IS2 measurements, they are most useful when combined with image type data. Specifically for ice services, the images used are satellite SAR images, and a combination of these data is encouraged.

https://doi.org/10.5194/tc-2020-315
Preprint. Discussion started: 29 October 2020

4 Conclusions

In this study, we have showed that it is possible to estimate the degree of ice ridging (DIR, in particular DIR2–DIR4) on sea ice using geolocated photons heights (ATL03) measured by IS2 during spring 2019 in the Bay of Bothnia. DIR derived from IS2 using our methodology follows the general expectations in the Baltic. This is the first time the feasibility of IS2 is studied from the viewpoint of winter navigation and operational ice charting. DIR is one of the most important parameters used in ice navigation as it indicates whether or not a vessel can safely pass through an ice-covered area. In the Baltic, daily ice charts provided by the FIS include information on DIR based primarily on *in situ* ice breaker observations and partly derived from SAR imagery.

Furthermore, we find that along-track densities of relative elevations (elevation anomaly, h_a, using the highest elevation subtracted the mean elevation within segments of 150 photons) above a threshold cut-off height of 0.4 m are consistent with the distributions of the DIR areas provided in the ice charts. Heavy deformation is found on sea ice close to the coast/fast ice regions, which is expected due to the sea ice drift pattern in the Baltic that pushes ice floes towards the coast causing deformation. Overall, we show that typical ridge densities and sail heights expected in the Bay of Bothnia correspond well to the elevation anomalies and the relationship of segments above and below the cut-off threshold.

In addition, this study demonstrates how much surface topography information of small-scale roughness ($<$1m) is measured by IS2 and kept, even when applying the high-confidence flag of the on-board filtering scheme. Thus, even over the thinner sea ice areas of the Baltic Sea (compared to the Arctic Ocean), one can benefit from the high density surface sampling and information that IS2 provides. We conclude that a time-critical IS2 product would be a tremendous benefit to ice services around the world complementing widely-used satellite SAR data.

Code and data availability. All data can be obtained by contacting the first author. ATL03 products were retrieved from NASA's Earth Search at https://search.earthdata.nasa.gov/. Ice charts were provided by the FIS. Shapefiles to produce map of Baltic Sea (Fig. 1) were provided by HELCOM, and is available for download at: http://maps.helcom.fi/website/mapservice/. Scripts used in the data analysis are available online at the following GitHub repository: https://github.com/reneefredensborg/DIR-from-IS2.

Author contributions. RFH, ER and HS conceived the concept of the study. Processing and computing was done by RFH. RFH, ER and HS jointly analysed the data, and SF joined in on discussions in relation to these analyses. RFH wrote the initial manuscript and all authors contributed to the editing of the text.

Competing interests. The authors declare that they have no competing interests.

https://doi.org/10.5194/tc-2020-315
Preprint. Discussion started: 29 October 2020

Acknowledgements. We thank FIS for providing their ice charts and expert advice, the Marine Research group at the Finnish Meteorological Institute for a great discussion and for interesting questions relevant to this study, and Kyle Duncan for useful insights on using IS2 for ridge detection in the Arctic.

https://doi.org/10.5194/tc-2020-315
Preprint. Discussion started: 29 October 2020

References

Abdalati, W., Zwally, H. J., Bindschadler, R., Csatho, B., Farrell, S. L., Fricker, H. A., Harding, D., Kwok, R., Lefsky, M., Markus, T., Marshak, A., Neumann, T., Palm, S., Schutz, B., Smith, B., Spinhirne, J., and Webb, C.: The ICESat-2 Laser Altimetry Mission, Proceedings of the IEEE, 98, 735–751, https://doi.org/10.1109/JPROC.2009.2034765, 2010.

Berglund, R. and Eriksson, P. B.: National ice service operations and products around the world, chap. 5.2, H. Shen (Ed.) Cold Regions Science and Marine Technology, "Ice Charts and – Formats", 2015.

BIM: Baltic Sea Icebreaking Report 2018-2019, Tech. rep., Baltic Icebreaking Management (BIM), available at: http://baltice.org/app/static/pdf/BIM%20Final%20Report%202019.pdf [Accessed 01 April 2020], 2019.

Brown, M. E., Arias, S. D., Neumann, T., Jasinksi, M. F., Posey, P., Babonis, G., Glenn, N. F., Birkett, C. M., Escobar, V. M., and Markus, T.: Applications for ICESat-2 Data, IEEE Geoscience and Remote Sensing Magazine, pp. 24–37, https://doi.org/10.1109/MGRS.2016.2560759, 2016.

Brunt, K. M., Neumann, T. A., and Smith, B. E.: Assessment of ICESat-2 Ice Sheet Surface Heights, Based on Comparisons Over the Interior of the Antarctic Ice Sheet, Geophysical Research Letters, 46, 13 072–13 078, https://doi.org/10.1029/2019GL084886, 2019.

Duncan, K., Farrell, S. L., Connor, L. N., Richter-Menge, J., Hutchings, J. K., and Dominguez, R.: High-resolution airborne observations of sea-ice pressure ridge sail height, Annals of Glaciology, 59, 137–147, https://doi.org/10.1017/aog.2018.2, 2018.

Farrell, S., Duncan, K., Buckley, E., Richter-Menge, J., and Li, R.: Mapping Sea Ice Surface Topography in High Fidelity with ICESat-2, Geophy. Res. Lett., p. 20, https://doi.org/10.1029/2020GL090708, accepted, 2020.

Farrell, S. L., Brunt, K. M., Ruth, J. M., Kuhn, J. M., Connor, L. N., and Walsh, K. M.: Sea-ice freeboard retrieval using digital photon.counting laser altimetry, Annals of Glaciology, 56, 167–174, https://doi.org/10.3189/2015AoG69A686, 2015.

Gegiuc, A., Similä, M., Karvonen, J., Lensu, M., Mäkynen, M., and Vainio, J.: Estimation of degree of sea ice ridging based on dual-polarized C-band SAR data, The Cryosphere, 12, 343–364, https://doi.org/10.5194/tc-12-343-2018, 2018.

Goerlandt, F., Goite, H., Banda, O. A. V., Höglund, A., Ahonen-Rainio, P., and Lensu, M.: An analysis of wintertime navigational accidents in the Northern Baltic Sea, Safety Science, 92, 66–84, https://doi.org/10.1016/j.ssci.2016.09.011, 2017.

Horvat, C., Blanchard-Wrigglesworth, E., and Petty, A.: Observing Waves in Sea Ice With ICESat-2, Geophysical Research Letters, 47, https://doi.org/10.1029/2020GL087629, 2020.

IMO: International code for ships operating in polar waters (Polar Code), Tech. rep., Internatinal Maritime Organisation (IMO), Marine Environment Protection Committee (MEPC), available at: http://www.imo.org/en/MediaCentre/HotTopics/polar/Documents/POLAR%20CODE%20TEXT%20AS%20ADOPTED.pdf [Accessed 17 August 2020], 2020.

Klotz, B. W., Neuenschwander, A., and Magruder, L. A.: High-Resolution Ocean Wave and Wind Characteristics Determined by the ICESat-2 Land Surface Algorithm, Geophysical Research Letters, 47, https://doi.org/10.1029/2019GL085907, 2020.

Kovacs, A., Weeks, W., Ackley, S., and Hibler, W.: Structure of a Multi-Year Pressure Ridge, Arctic, 26, 22–31, https://doi.org/10.14430/arctic2893, 1973.

Kwok, R., Kacimi, S., Markus, T., Kurtz, N. T., Studinger, M., Sonntag, J. G., Manizade, S. S., Boisvert, L. N., and Harbeck, J. P.: ICESat-2 Surface Height and Sea Ice Freeboard Assessed with ATM Lidar Acquisitions From Operation IceBridge, Geophysical Research Letters, 46, 11 228–11 236, https://doi.org/10.1029/2019GL084976, 2019a.

https://doi.org/10.5194/tc-2020-315
Preprint. Discussion started: 29 October 2020

Kwok, R., Markus, T., Kurtz, N. T., Neumann, T. A., Farrell, S. L., Cunningham, C. F., Hancock, D. W., Ivanoff, A., and Wimert, J. T.: Surface Height and Sea Ice Freeboard of the Arctic Ocean from ICESat-2: Characteristics and Early Results, Journal of Geophysical Research: Oceans, 124, 6942–6959, https://doi.org/10.1029/2019JC015486, 2019b.

Lewis, J., Leppäranta, M., and Granberg, H.: Statistical properties of sea ice surface topography in the Baltic Sea, Tellus, 45A, 127–142, 1993.

Leys, C., Ley, C., Klein, O., Bernard, P., and Licata, L.: Detecting outliers: Do not use standard deviation around the mean, use absolute deviation around the median, Journal of Experimental Social Psychology, 49, 764–766, https://doi.org/10.1016/j.jesp.2013.03.013, 2013.

Markus, T., Neumann, T., Martino, A., Abdalati, W., Brunt, K., Csatho, B., Farrell, S., Fricker, H., Gardner, A., Harding, D., Jasinksi, M., Kwok, R., Magruder, L., Lubin, D., Lutchke, S., Morison, J., Nelson, R., Neuenschwander, A., Palm, S., Popescu, S., Schum, C., Schutz, B. E., Smith, B., Yang, Y., and Zwally, J.: The Ice, Cloud and land Elevation Satellite-2 (ICESat-2): Science requirements, concept and implementation, Remote Sensing of Environment, 190, 260–273, https://doi.org/10.1016/j.rse.2016.12.029, 2017.

Melia, N., Haines, K., and Hawkins, E.: Sea ice decline and 21st centurytrans-Arctic shipping routes, Geophysical Research Letter, 43, 9720–9728, https://doi.org/10.1002/2016GL069315, 2016.

Neumann, T. A., Martino, A. J., Markus, T., Bae, S., Bock, M. R., Brenner, A. C., Brunt, K. M., Cavanaugh, J., Fernandes, S. T., Hancock, D. W., Harbeck, K., Lee, J., Kurtz, N. T., Luers, P. J., Lutchke, S. B., Magruder, L., Pennington, T. A., Ramos-Izquierdo, L., Rebold, T., Skoog, J., and Thomas, T. C.: The Ice, Cloud and Land Elevation Satellite - 2 mission: A global geolocated photon product derived from the Advanced Topographic Laser Altimeter System, Remote Sensing of Environment, 233, 16, https://doi.org/10.1016/j.rse.2019.111325, 2019.

Ronkainen, I., Lehtiranta, J., Lensu, M., Rinne, E., Haapala, J., and Haas, C.: Interannual sea ice thickness variability in the Bay of Bothnia, The Cryosphere, 12, 3459–3476, https://doi.org/10.5194/tc-12-3459-2018, 2018.

WMO: Sea-Ice Information Services in the World, vol. 574, 2010 edn., World Meteorological Organisation (WMO), 2010.